

The weak strangeness production reaction $pn \rightarrow p\Lambda$ in a one-boson-exchange model

A. Parreño *, A. Ramos

*Departament d'Estructura i Constituents de la Matèria, Universitat de Barcelona,
Diagonal 647, 08028 Barcelona, Spain*

N.G. Kelkar

Nuclear Physics Division, Bhabha Atomic Research Centre, Trombay, Mumbai-400 085, India

C. Bennhold

*Center of Nuclear Studies, Department of Physics, The George Washington University,
Washington, DC 20052, USA*

Abstract

The weak production of Lambdas in nucleon-nucleon scattering is studied in a meson-exchange framework. The weak transition operator for the $NN \rightarrow N\Lambda$ reaction is identical to a previously developed weak strangeness-changing transition potential $\Lambda N \rightarrow NN$ that describes the nonmesonic decay of hypernuclei. The initial NN and final YN state interaction has been included by using realistic baryon-baryon forces that describe the available elastic scattering data. The total and differential cross sections as well as the parity-violating asymmetry are studied for the reaction $pn \rightarrow p\Lambda$. These observables are found to be sensitive to the opening of the Σ production channel, the choice of the strong interaction potential and the structure of the weak transition potential.

*Present address: INT, University of Washington, Seattle, WA 98195

I. INTRODUCTION

Over the last several decades, the Standard Model of weak interactions has been thoroughly tested by a vast amount of data for leptonic and semi-leptonic decays and reactions. Hadronic weak interactions are in general more difficult to study experimentally since they are usually obscured by the presence of the much larger strong interaction. This requires employing processes in which the strong force cannot participate due to overriding symmetry principles. In the case of the weak nucleon-nucleon interaction it was realized more than 40 years ago [1] that the current-current form of the weak interaction dictates the presence of a weak transition between nucleons which would lead to parity impurities in nuclear states which are of first order in the weak coupling. Using these parity nonconserving observables in many experiments on nuclear gamma and alpha transitions, polarized NN scattering, as well as the recent first measurement of the nuclear anapole moment [2], much has been learned about the weak nucleon-nucleon interaction [3].

The situation is very different for the flavor-changing baryon-baryon interaction. Soon after the discovery of hypernuclei it was recognized that the Λ inside the nuclear medium decays not through its Pauli-blocked mesonic decay channel, but predominantly through the $\Delta S = 1$ nonmesonic transition $\Lambda N \rightarrow NN$, thus opening a door to the study of the weak strangeness-changing hyperon-nucleon force. However, experimental progress in this field of weak hypernuclear decays has been slow until recently due to the difficult multi-coincidence, low count-rate nature of these measurements. In recent years the situation has improved significantly due to a series of new experiments at BNL and KEK. On the theoretical side it became clear that in order to unambiguously extract the weak $\Lambda N \rightarrow NN$ transition potential significant effort must be spent to account for the nuclear structure effects as accurately as possible. When this task was recently completed [4] it became apparent that major discrepancies between theory and experiment cannot be due to the underlying nuclear structure but have to arise from the nature of the weak transition potential itself.

Even with the nuclear structure input under control it has become desirable to measure

the process $NN \rightarrow N\Lambda$ directly since the hypernuclear decay can only probe the reaction at one well-defined kinematic setting. Though considered impossible for many years since this process is reduced in cross section by around 12 orders of magnitude from the standard elastic NN scattering, recent progress in experimental and accelerator technology may have brought measuring this process within reach [5]. It is therefore timely to provide predictions of various observables based on the transition potential used in the nonmesonic hypernuclear decay.

In Sec. II of this paper, we present the expressions for the matrix elements and the cross section. Sec. III briefly describes the transition operator derived in Ref. [4]. Our results are discussed in Sec. IV and summarized in Sec. V.

II. DIFFERENTIAL CROSS-SECTION

The differential cross section per unit solid angle in the center-of-mass system for the reaction $pn \rightarrow p\Lambda$ as depicted in Fig. 1 is given by the expression

$$\frac{d\sigma}{d\Omega} = (2\pi)^4 \frac{1}{s} \frac{|\vec{p}_F|}{|\vec{p}_I|} E_1 E_2 E_3 E_4 \frac{1}{(2s_1 + 1)(2s_2 + 1)} \sum_{m_{s_1}} \sum_{m_{s_2}} \sum_{m_{s_3}} \sum_{m_{s_4}} |\mathcal{M}_{FI}|^2, \quad (1)$$

with $\sqrt{s} = E_1 + E_2 = E_3 + E_4$ the total available energy in the center-of-mass system and \vec{p}_I and \vec{p}_F the relative momenta of the particles in the initial and final states respectively. In a plane wave Born approximation (PWBA) the weak transition matrix elements read

$$\mathcal{M}_{FI} = \langle \vec{p}_3 m_{s_3} t_3, \vec{p}_4 m_{s_4} t_4 | V^w \overline{|\vec{p}_1 m_{s_1} t_1, \vec{p}_2 m_{s_2} t_2\rangle} \rangle \quad (2)$$

where the overline stands for the antisymmetric combination of the two particle states $\{1\}$ and $\{2\}$ and V^w is the nonrelativistic weak transition potential.

Accounting for the locality of the weak potential, the direct term of the previous matrix elements can be written in the distorted wave Born approximation (DWBA) as

$$\mathcal{M}_{FI} = \sum_{S_F M_{S_F}} \sum_{S_I M_{S_I}} \sum_{T M_T} \langle \frac{1}{2} m_{s_3} \frac{1}{2} m_{s_4} | S_F M_{S_F} \rangle \langle \frac{1}{2} t_3 \frac{1}{2} t_4 | T M_T \rangle$$

$$\begin{aligned}
& \times \langle \frac{1}{2} m_{s_1} \frac{1}{2} m_{s_2} | S_I M_{S_I} \rangle \langle \frac{1}{2} t_1 \frac{1}{2} t_2 | T M_T \rangle \\
& \times \int d\Omega \int r^2 dr [\Psi_{\Lambda N}^{(-)}(\vec{p}_F, \vec{r})]^* \chi_{M_T}^{\dagger T} V^w(\vec{r}) \Psi_{NN}^{(+)}(\vec{p}_I, \vec{r}) \chi_{M_T}^T
\end{aligned} \tag{3}$$

where $V^w(\vec{r})$ contains the radial, angular and isospin dependence of the weak transition potential and $\Psi_{\Lambda N}^{(-)}$ ($\Psi_{NN}^{(+)}$) stands for the distorted ΛN (NN) wave function.

In Sec. III it is shown how the weak potential can be decomposed as

$$V^w(\vec{r}) = \sum_i \sum_{\alpha} V_{\alpha}^{(i)}(\vec{r}) = \sum_i \sum_{\alpha} V_{\alpha}^{(i)}(r) V_{\alpha}^{(i)}(\hat{r}) \hat{I}_{\alpha}^{(i)}, \tag{4}$$

where the index i sums over mesons and α over the different spin channels. The radial part of the potential is denoted by $V_{\alpha}^{(i)}(r)$, the piece containing the angular and spin dependence by $V_{\alpha}^{(i)}(\hat{r})$ and $\hat{I}_{\alpha}^{(i)}$ denotes the appropriate isospin operator for each meson.

Using the partial wave decomposition for the distorted waves, working in the coupled basis formalism, $LS(J)$ (see appendix), and assuming \hat{p}_I parallel to the z-axis, the modulus squared of the weak matrix elements for the $pn \rightarrow p\Lambda$ reaction finally reads

$$\begin{aligned}
|\mathcal{M}_{FI}|^2 &= \sum_{S_F M_{S_F}} \sum_{S_I M_{S_I}} \sum_T \langle \frac{1}{2} t_1 \frac{1}{2} t_2 | T 0 \rangle^2 \langle T 0 | \frac{1}{2} t_3 \frac{1}{2} t_4 \rangle^2 \\
& \times \left| \frac{2}{\pi} \sum_i \sum_{\alpha} \langle T 0 | I_{\alpha}^{(i)} | T 0 \rangle \sum_J \sum_{L'_F S'_F} \sum_{L_F} \sum_{L_I} \sum_{L'_I} i^{(L'_I - L'_F)} \right. \\
& \times \langle L_F M_{L_F} S_F M_{S_F} | J M \rangle Y_{L_F M_{L_F}}(\hat{p}_F) \langle L_I M_{L_I} S_I M_{S_I} | J M_{S_I} \rangle \sqrt{\frac{2L_I + 1}{4\pi}} \\
& \times \int r^2 dr [\psi_{\Lambda N}^{(-)*}]_{L'_F S'_F, L_F S_F}^J(k_F, r) V_{\alpha}^{(i)}(r) [\psi_{NN}^{(+)}]_{L'_I S_I, L_I S_I}^J(k_I, r) \\
& \times \left. \int d\Omega \mathcal{J}_{L'_F S'_F}^{\dagger JM}(\hat{r}) V_{\alpha}^{(i)}(\hat{r}) \mathcal{J}_{L'_I S'_I}^{JM}(\hat{r}) \left(\frac{1 - (-1)^{L'_I + S_I + T}}{\sqrt{2}} \right) \right|^2.
\end{aligned} \tag{5}$$

The distorted radial wave functions in the above equation are generated from a T-matrix which is constructed using the nucleon-nucleon (NN) and hyperon-nucleon (YN) strong potentials. We make use of the Nijmegen 93 [6] and Bonn B [7] NN potentials and the Nijmegen soft-core [8] and Jülich [9] YN potentials. Comparison between the results obtained using the different interaction models is made in Sec. IV.

III. THE WEAK POTENTIAL

In Ref. [4] a one-boson-exchange model is developed to describe the $\Lambda N \rightarrow NN$ transition, where the pseudoscalar π, η, K and vector ρ, ω and K^* mesons mediate the interaction. We use this model in order to describe the present inverse reaction. In this study we have refrained from considering the transition $pn \rightarrow N\Sigma \rightarrow p\Lambda$, since it was found to be an order of magnitude smaller than that for the direct Λ production [10].

The nonrelativistic reduction of the Feynman amplitude, corresponding to the diagram depicted in Fig. 1, leads to the nonrelativistic weak potential in momentum space, which for the exchange of pseudoscalar mesons takes the form

$$V_{ps}^w(\vec{q}) = -G_F m_\pi^2 \frac{g}{2M_N} \left(\hat{A} + \frac{\hat{B}}{2\overline{M}} \vec{\sigma}_1 \vec{q} \right) \frac{\vec{\sigma}_2 \vec{q}}{\vec{q}^2 + \mu^2}, \quad (6)$$

where $G_F m_\pi^2 = 2.21 \times 10^{-7}$ is the Fermi coupling constant, \vec{q} is the momentum carried by the meson (M) directed towards the strong vertex, $g = g_{NNM}$ the strong coupling constant for the NNM vertex, μ the meson mass, M_N the nucleon mass and \overline{M} the average between the nucleon and Λ masses. The operators \hat{A} and \hat{B} contain, in addition to the weak coupling constants, the particular isospin structure corresponding to the exchanged meson.

In the case of vector meson exchange the weak potential takes the form

$$V_v^w(\vec{q}) = G_F m_\pi^2 \left(F_1 \hat{\alpha} - \frac{(\hat{\alpha} + \hat{\beta})(F_1 + F_2)}{4M_N \overline{M}} (\vec{\sigma}_1 \times \vec{q})(\vec{\sigma}_2 \times \vec{q}) + i \frac{\hat{\varepsilon}(F_1 + F_2)}{2M_N} (\vec{\sigma}_1 \times \vec{\sigma}_2) \vec{q} \right) \frac{1}{\vec{q}^2 + \mu^2}, \quad (7)$$

with $F_1 = g_{NNM}^V$, $F_2 = g_{NNM}^T$ the strong coupling constants and $\hat{\alpha}$, $\hat{\beta}$ and $\hat{\varepsilon}$ the weak coupling constants that also contain the appropriate isospin operator of the particular meson.

Performing a Fourier transform of Eqs. (6) and (7), and using the relation $(\vec{\sigma}_1 \times \vec{q})(\vec{\sigma}_2 \times \vec{q}) = (\vec{\sigma}_1 \vec{\sigma}_2) \vec{q}^2 - (\vec{\sigma}_1 \vec{q})(\vec{\sigma}_2 \vec{q})$ in (7), one obtains the weak transition potential in coordinate space, which can be cast into the form

$$V^w(\vec{r}) = \sum_i \sum_\alpha V_\alpha^{(i)}(\vec{r}) = \sum_i \sum_\alpha V_\alpha^{(i)}(r) V_\alpha^{(i)}(\hat{r}) \hat{I}_\alpha^{(i)}$$

$$\begin{aligned}
&= \sum_i \left[V_C^{(i)}(r) \hat{I}_C^{(i)} + V_{SS}^{(i)}(r) \vec{\sigma}_1 \vec{\sigma}_2 \hat{I}_{SS}^{(i)} + V_T^{(i)}(r) S_{12}(\hat{r}) \hat{I}_T^{(i)} + \right. \\
&\quad \left. + \left(n^i \vec{\sigma}_2 \cdot \hat{r} + (1 - n^i) [\vec{\sigma}_1 \times \vec{\sigma}_2] \cdot \hat{r} \right) V_{PV}^{(i)}(r) \hat{I}_{PV}^{(i)} \right] , \tag{8}
\end{aligned}$$

where the index i runs over the different mesons exchanged ($i = 1, \dots, 6$ represents $\pi, \eta, K, \rho, \omega, K^*$) and α over the different spin operators denoted by C (central spin independent), SS (central spin dependent), T (tensor) and PV (parity violating). In the above expression, $n^i = 1(0)$ refers to the pseudoscalar (vector) mesons. In the case of isovector mesons (π, ρ) the isospin factor is $\vec{\tau}_1 \vec{\tau}_2$ and for isoscalar mesons (η, ω) this factor is just $\hat{1}$ for all spin structure pieces of the potential. In the case of isodoublet mesons (K, K^*) there are contributions proportional to $\hat{1}$ and to $\vec{\tau}_1 \vec{\tau}_2$ that depend on the coupling constants and, therefore, on the spin structure piece of the potential denoted by α . For K -exchange we have

$$\begin{aligned}
\hat{I}_C^{(3)} &= 0 \\
\hat{I}_{SS}^{(3)} &= \hat{I}_T^{(3)} = \frac{C_K^{PC}}{2} + D_K^{PC} + \frac{C_K^{PC}}{2} \vec{\tau}_1 \vec{\tau}_2 \\
\hat{I}_{PV}^{(3)} &= \frac{C_K^{PV}}{2} + D_K^{PV} + \frac{C_K^{PV}}{2} \vec{\tau}_1 \vec{\tau}_2 , \tag{9}
\end{aligned}$$

and for K^* -exchange

$$\begin{aligned}
\hat{I}_C^{(6)} &= \frac{C_{K^*}^{PC,V}}{2} + D_{K^*}^{PC,V} + \frac{C_{K^*}^{PC,V}}{2} \vec{\tau}_1 \vec{\tau}_2 \\
\hat{I}_{SS}^{(6)} &= \hat{I}_T^{(6)} = \frac{(C_{K^*}^{PC,V} + C_{K^*}^{PC,T})}{2} + (D_{K^*}^{PC,V} + D_{K^*}^{PC,T}) + \frac{(C_{K^*}^{PC,V} + C_{K^*}^{PC,T})}{2} \vec{\tau}_1 \vec{\tau}_2 \\
\hat{I}_{PV}^{(6)} &= \frac{C_{K^*}^{PV}}{2} + D_{K^*}^{PV} + \frac{C_{K^*}^{PV}}{2} \vec{\tau}_1 \vec{\tau}_2 . \tag{10}
\end{aligned}$$

The different pieces $V_\alpha^{(i)}(r)$, with $\alpha = C, SS, T, PV$, are given by

$$V_C^{(i)}(r) = K_C^{(i)} \frac{e^{-\mu_i r}}{4\pi r} \equiv K_C^{(i)} V_C(r, \mu_i) \tag{11}$$

$$V_{SS}^{(i)}(r) = K_{SS}^{(i)} \frac{1}{3} \left[\mu_i^2 \frac{e^{-\mu_i r}}{4\pi r} - \delta(\vec{r}) \right] \equiv K_{SS}^{(i)} V_{SS}(r, \mu_i) \tag{12}$$

$$V_T^{(i)}(r) = K_T^{(i)} \frac{1}{3} \mu_i^2 \frac{e^{-\mu_i r}}{4\pi r} \left(1 + \frac{3}{\mu_i r} + \frac{3}{(\mu_i r)^2} \right) \equiv K_T^{(i)} V_T(r, \mu_i) \tag{13}$$

$$V_{PV}^{(i)}(r) = K_{PV}^{(i)} \mu_i \frac{e^{-\mu_i r}}{4\pi r} \left(1 + \frac{1}{\mu_i r} \right) \equiv K_{PV}^{(i)} V_{PV}(r, \mu_i) . \tag{14}$$

where μ_i denotes the mass of the different mesons. The expressions for $K_\alpha^{(i)}$, which contain factors and coupling constants, are given in Table I. The explicit values of the coupling constants can be found in Table III of Ref. [4].

A monopole form factor $F_i(\vec{q}^2) = (\Lambda_i^2 - \mu_i^2)/(\Lambda_i^2 + \vec{q}^2)$ is used at each vertex, where the value of the cut-off, Λ_i , depends on the meson. These values are the same ones as those of the strong Jülich YN interaction [9], since the Nijmegen model distinguishes form factors only in terms of the transition channel. The resulting expressions for the regularized potentials, which were given already in Ref. [4], will be repeated here in order to correct for some misprints. The effect of form factors is included by making the following replacements in Eqs. (11) to (14)

$$V_C(r; \mu_i) \rightarrow V_C(r; \mu_i) - V_C(r; \Lambda_i) - \frac{\Lambda_i^2 - \mu_i^2}{2\Lambda_i} \frac{e^{-\Lambda_i r}}{4\pi} \quad (15)$$

$$V_{SS}(r; \mu_i) \rightarrow V_{SS}(r; \mu_i) - V_{SS}(r; \Lambda_i) - \Lambda_i \frac{\Lambda_i^2 - \mu_i^2}{6} \frac{e^{-\Lambda_i r}}{4\pi} \left(1 - \frac{2}{\Lambda_i r}\right) \quad (16)$$

$$V_T(r; \mu_i) \rightarrow V_T(r; \mu_i) - V_T(r; \Lambda_i) - \Lambda_i \frac{\Lambda_i^2 - \mu_i^2}{6} \frac{e^{-\Lambda_i r}}{4\pi} \left(1 + \frac{1}{\Lambda_i r}\right) \quad (17)$$

$$V_{PV}(r; \mu_i) \rightarrow V_{PV}(r; \mu_i) - V_{PV}(r; \Lambda_i) - \frac{\Lambda_i^2 - \mu_i^2}{2} \frac{e^{-\Lambda_i r}}{4\pi} . \quad (18)$$

IV. RESULTS

The total cross section for the $pn \rightarrow p\Lambda$ reaction including only one-pion-exchange in the weak transition potential is shown in Fig. 2 as a function of the proton lab momentum, starting at the $p\Lambda$ threshold. As expected for a weak process, the cross section is of the order of 10^{-12} mb. The dashed line corresponds to the “free” calculation where form factors are omitted at the vertices and the incoming pn and outgoing $p\Lambda$ states propagate as plane waves. The thin solid line includes form factors and strong initial pn distorted waves obtained from the Nijmegen 93 NN interaction [6]. The effect of the NN interaction is to reduce the cross section by a factor of about 2. The reduction is a result of the fact that the pn pair moves with large relative momentum (from 415 MeV/c to 525 MeV/c) in the range

of proton lab momenta explored and feels the effect of the strong repulsive short range part of the NN interaction. As a consequence, the pn wave function is much reduced at small distances where the weak transition potential contributes most to the cross section and hence the cross section becomes smaller. The thick solid line shows the cross section when the $p\Lambda$ distortions, obtained from the YN Nijmegen Soft Core potential [8], are also included. When compared to the thin line, one observes a substantial enhancement of the cross section in the low momentum region which turns into a moderate reduction at high lab momentum values. This is due to the fact that, close to threshold, the $p\Lambda$ pair moves with small relative momentum, feeling the attractive component of the YN potential. As a result the wave function gets pushed in to smaller distances and the cross section is enhanced. As the proton lab momentum increases, so does the relative $p\Lambda$ momentum and, eventually, the repulsive core of the YN interaction becomes responsible for reducing the wave function at short distances, giving rise to smaller cross sections. The opening of the ΣN channel, coupled to the ΛN one through the strong interaction, shows up as a step in the cross section at a proton lab momentum around 1140 MeV/c.

The effect of including the different mesons in the weak transition potential is shown in Fig. 3. Fig. 3a shows the cross sections calculated using the Nijmegen potentials for getting the NN and ΛN distorted waves and Fig. 3b shows those using the Bonn B NN and Jülich A ΛN potentials. In Fig. 3a we see that adding the ρ meson to one-pion-exchange considerably reduces the cross section in the kinematic region studied here. Including the remaining mesons does not change the cross section much, which ends up being about a factor 2 smaller than that for one-pion only. This effect appears to be surprisingly different from the moderate reduction of 15% found for the decay rate of hypernuclei when the effect of adding heavier mesons to the one-pion-exchange mechanism was studied [4]. However, we point out that the ΛN correlations in the weak hypernuclear decay case were obtained from a G-matrix calculation which takes into account the Pauli principle acting on the intermediate nucleon. This blocks the low relative momentum transitions between the initial ΛN and intermediate YN states and, therefore, the effect of the attractive part of the interaction

on the correlated ΛN wave function is much reduced compared to those of the distorted $p\Lambda$ wave function in free space. Thus, the ΛN wave function in the hypernucleus is strongly suppressed at small distances, making the contribution of the heavier mesons less important.

As can be seen in Fig. 3b, the use of the Bonn B NN and Jülich A ΛN potentials give rise to different effects in the cross section as compared to those calculated using the Nijmegen ones. Although not shown in the figures, we have checked that, in the absence of $p\Lambda$ distortions, the cross section calculated with the distorted pn waves, obtained from either the Nijmegen 93 or the Bonn B potentials, yield nearly identical results. Therefore, the differences between the results in Figs. 3a and 3b come almost completely from the different models used to distort the $p\Lambda$ final state. Already at the level of only pion-exchange (dashed line in Fig. 3b), the Jülich A model shows a clear enhancement close to the $p\Sigma$ threshold. Adding the ρ meson furthermore yields a strong reduction of the cross section. On the other hand, the addition of the remaining mesons produces a substantial enhancement which gives rise to a final cross section not very different from the pion-only result. We note here that the pion-only cross section shown in Fig. 3 is close to the results obtained in Ref. [10] with one-pion-exchange, but we do not find the tremendous enhancement of a factor of 3 in the cross section when the ρ meson is included. This is most likely due to the different models for the weak $\rho N\Lambda$ vertices used in the ρ -exchange mechanism. Their weak coupling constants are larger than the ones used here by a factor of more than 2 for the parity conserving ones (α_ρ and β_ρ) and a factor 3.5 for the parity violating one (ε_ρ).

Let us now explore the origin of the peak in the cross section around the Σ threshold. Nuclear matter calculations already showed some time ago [11–13] that, while the Λ binding energy in nuclear matter turned out to be about -25 to -30 MeV for the Nijmegen and Jülich interactions, the distribution of this strength between the various partial waves was very different. The most important contribution for the Jülich interactions came from the coupled ${}^3S_1 - {}^3D_1$ channel, the 1S_0 contribution being negligible. However, the Nijmegen interactions obtained almost equal contributions from both the $J = 0$ and $J = 1$ channels. In Fig. 4 we analyze the contribution to the $pn \rightarrow p\Lambda$ cross section from ${}^3S_1 - {}^3D_1$ partial waves

obtained from the Nijmegen (Fig. 4a) and Jülich A (Fig. 4b) ΛN interactions. The thick solid lines (“full”) are the calculated cross sections with one-pion-exchange for the weak transition $pn \rightarrow p\Lambda$ and including distorted waves for the pn and $p\Lambda$ systems. The short dashed lines represent cross sections obtained by removing the ${}^3S_1 \rightarrow {}^3S_1$ component of the distorted $p\Lambda$ wave function and the long-dashed lines those obtained when the ${}^3D_1 \rightarrow {}^3D_1$ component is removed. The thin solid line shows the small cross sections obtained when all the ${}^3S_1 - {}^3D_1$ coupled channel is omitted, thus reflecting the fact that these are the most important components for the $pn \rightarrow p\Lambda$ reaction, as already noted in Ref. [10]. The stronger ${}^3S_1 - {}^3D_1$ channel of the Jülich interaction, relative to the Nijmegen one, is the reason for the much more enhanced cross section at the $N\Sigma$ threshold. Suppressing the 1S_0 partial waves barely affects the cross section and cannot be seen in Figs. 4a and 4b. In spite of the fact that the Nijmegen YN interaction has a sizable 1S_0 component, its contribution to the cross section gets eliminated due to the weak one-pion-exchange transition potential which has negligible strength for the ${}^1S_0 \rightarrow {}^1S_0$ transition.

In Fig. 5 we show the differential cross sections for the proton lab momentum of 1137 MeV/c which corresponds to the position of the peak in Fig. 3, where the strong NN and ΛN correlations have been generated with the Bonn B and Jülich A interactions, respectively. The dashed line is the result for the pion-only calculation, the thin solid line shows the effect of including the ρ meson and the thick solid line incorporates the full set of six mesons. The effect of adding the rho to the pion is a reduction of a factor slightly more than 2 while adding all mesons brings the results closer to the one-pion ones, as observed earlier for the total cross section.

A measure of the amount of parity violation in the weak Λ production is given by the asymmetry A defined as

$$A = \frac{\sigma_+ - \sigma_-}{\sigma_+ + \sigma_-}, \quad (19)$$

where σ_+ (σ_-) is the cross section for positive (negative) helicity of the incoming proton. In Fig. 6 we consider the one-pion-exchange mechanism in the weak $pn \rightarrow p\Lambda$ transition and

illustrate the effect of the strong distortions on the asymmetry A using the Nijmegen models for the NN and ΛN interactions. The dashed line shows the asymmetry when neither the form factors at the vertices nor the strong distortions are included. The inclusion of the NN interactions, as shown by the thin solid line, decrease the value of the asymmetry up to a beam momentum of 1130 MeV/c beyond which it increases compared to the dashed line. The addition of the ΛN final state interaction gives rise to the particular cusp structure due to the opening of the ΣN channel around 1140 MeV/c.

The effect of the different meson exchanges in the weak transition potential is shown in Fig. 7 where the NN and ΛN distorted waves have been generated with the Bonn B and Jülich A models, respectively. We observe that while the ρ meson increases the asymmetry with respect to the pion-only result, the inclusion of all the six mesons produces an asymmetry which is considerably smaller. Similar qualitative features are found when the Nijmegen potential models are used in constructing the distorted NN and ΛN waves.

Finally, we present in Figs. 8a and 8b the $pn \rightarrow p\Lambda$ cross sections and asymmetries, respectively, obtained with the full meson-exchange weak transition potential for three different strong interaction models. The dashed lines use the NN Nijmegen 93 and YN Nijmegen Soft Core models, the thin solid lines use the NN Bonn B and YN Jülich B models and the thick solid lines use the NN Bonn B and the YN Jülich A models. As mentioned before, the differences between the curves are mainly due to the differences in the YN potentials employed.

It is clear that these strong YN potentials are not sufficiently constrained by the small amount of total cross section data on YN scattering. Hence the different YN models which produce the total cross sections for YN scattering equally well, give rise to very different predictions when applied to other reactions that are sensitive to the YN interaction, like hypernuclear structure calculations, studies of nuclear matter with strangeness, or the weak transition $pn \rightarrow p\Lambda$ studied here. More data on YN scattering, especially on differential cross sections and polarization observables, is highly desirable in order to constraint the YN interactions sufficiently well so that the $pn \rightarrow p\Lambda$ reaction can be used to learn about the

weak four fermion interaction. In particular, the two-step $pn \rightarrow N\Sigma \rightarrow p\Lambda$ transition, not considered in the present work, could be studied after having a better knowledge of the YN interaction.

V. SUMMARY

We have studied the weak strangeness production reaction $pn \rightarrow p\Lambda$ in a distorted wave Born approximation formalism using the one-meson-exchange model for the weak transition consisting of six mesons viz. the $\pi, \rho, \eta, \omega, K$ and K^* . The distorted wave functions are written in terms of partial wave expansions and are generated using the different available potentials for nucleon-nucleon and hyperon-nucleon interactions.

The total cross sections are sensitive to the model ingredients of the weak transition operator. Including the ρ meson decreases the pion-only cross sections by a factor of 2 or more. The effect of the remaining mesons depends on the strong potentials employed to distort the $p\Lambda$ states, giving rise to cross sections that can be either very close or a factor 2 smaller than the pion-only results.

The kinematical region explored by the free $pn \rightarrow p\Lambda$ reaction is much larger than that by the inverse reaction, the nonmesonic decay $\Lambda N \rightarrow NN$ taking place inside hypernuclei. The heavier mesons contribute very differently and are more important in the free reaction compared to the nonmesonic decay due to the different behavior of the ΛN wave function inside a hypernucleus compared to that in free space.

The total cross section computed with the Nijmegen ΛN wave functions show a step-like behavior around 1140 MeV/c beam momentum, where the strong $\Lambda N \rightarrow \Sigma N$ transition opens up. The Jülich ΛN results show a dramatic peak in this region. However, the peak in our results is not as pronounced as the one found in earlier work [10]. The major contribution to these cross sections comes from the ΛN partial waves in the ${}^3S_1 - {}^3D_1$ coupled channels.

We find the $pn \rightarrow p\Lambda$ reaction to be very sensitive to the type of model used for the strong hyperon-nucleon interaction. Hence, more data on YN scattering for observables

other than the total cross sections are needed to constrain the YN interaction models and use the $pn \rightarrow \Lambda p$ reaction to extract the weak four fermion interaction.

The cross sections for the $pn \rightarrow p\Lambda$ reaction are of the order of 10^{-12} mb and are at the borderline of feasibility for the existing experimental facilities.

VI. ACKNOWLEDGEMENTS

This work is partially supported by the DGICYT contract No. PB95-1249 (Spain), the Generalitat de Catalunya grant No. GRQ94-1022, the US-DOE grant No. DE-FG02-95-ER40907 and the NATO grant No. CRG960132. One of the authors (N.G.K.) would like to thank the warm hospitality of the nuclear physics group at the University of Barcelona.

VII. APPENDIX

The Lippmann-Schwinger equation allows us to obtain the scattered wave function for a pair of particles moving under the influence of the strong interaction. The scattered states will then be given by

$$|\Psi_{NN}^{(+)}\rangle = |\Phi_{NN}\rangle + \frac{1}{E_{NN} - H_{0NN} + i\eta} T_{NN} |\Phi_{NN}\rangle \quad (20)$$

for the incoming NN states and by

$$\langle\Psi_{\Lambda N}^{(-)}| = \langle\Phi_{\Lambda N}| + \langle\Phi_{\Lambda N}| T_{\Lambda N} \frac{1}{E_{\Lambda N} - H_{0\Lambda N} + i\eta} \quad (21)$$

for the outgoing ΛN states. The previous equations are written in terms of the T-matrix which is obtained from

$$T = V + V \frac{1}{E - H_0 + i\eta} T \quad (22)$$

and fulfills

$$V_{NN} |\Psi_{NN}^{(+)}\rangle = T_{NN} |\Phi_{NN}\rangle \quad (23)$$

$$V_{\Lambda N} |\Psi_{\Lambda N}^{(-)}\rangle = T_{\Lambda N}^{\dagger} |\Phi_{\Lambda N}\rangle \quad (24)$$

$|\Phi_{NN}\rangle$ and $|\Phi_{\Lambda N}\rangle$ being the corresponding unperturbed states for the NN and ΛN systems, respectively. Note that Eq. (24) should have been written as

$$V_{\Lambda N \rightarrow \Lambda N} |\Psi_{\Lambda N \rightarrow \Lambda N}^{(-)}\rangle + V_{\Sigma N \rightarrow \Lambda N} |\Psi_{\Sigma N \rightarrow \Lambda N}^{(-)}\rangle = T_{\Lambda N \rightarrow \Lambda N}^{\dagger} |\Phi_{\Lambda N \rightarrow \Lambda N}\rangle \quad (25)$$

However, since we disregard the $pn \rightarrow N\Sigma \rightarrow p\Lambda$ transition, we don't need to consider the $\Sigma N \rightarrow \Lambda N$ component of the wave function, $|\Psi_{\Sigma N \rightarrow \Lambda N}^{(-)}\rangle$. Simplifying the notation by writing $\Lambda N \rightarrow \Lambda N$ as simply ΛN Eq. (25) finally reduces to Eq. (24).

Projecting Eqns. (20) and (21) into \vec{r} -space and performing a partial-wave decomposition, the distorted waves can be written as

$$\begin{aligned} [\Psi_{\vec{p}_F, S_F M_{S_F}}^{(-)\Lambda N}(\vec{r})]^* \chi_{M_T}^{\dagger} &= \sqrt{\frac{2}{\pi}} \sum_{JM} \sum_{L'_F S'_F} \sum_{L_F M_{L_F}} (-i)^{L'_F} [\psi_{\Lambda N}^{(-)}]_{L'_F S'_F, L_F S_F}^{*J}(\vec{p}_F, r) \\ &\times \langle L_F M_{L_F} S_F M_{S_F} | JM \rangle Y_{L_F M_{L_F}}(\hat{p}_F) \mathcal{J}_{L'_F S'_F}^{JM}(\hat{r}) \end{aligned} \quad (26)$$

and

$$\begin{aligned} \Psi_{\vec{p}_I, S_I M_{S_I}}^{(+)\, NN}(\vec{r}) \chi_{M_T}^T &= \sqrt{\frac{2}{\pi}} \sum_{JM} \sum_{L'_I} \sum_{L_I M_{L_I}} i^{L'_I} [\psi_{NN}^{(+)}]_{L'_I S_I, L_I S_I}^J(p_I, r) \\ &\quad \langle L_I M_{L_I} S_I M_{S_I} | JM \rangle Y_{L_I M_{L_I}}^*(\hat{p}_I) \mathcal{J}_{L'_I S_I}^{JM}(\hat{r}) \end{aligned} \quad (27)$$

where the quantities $\mathcal{J}_{L'S}^{JM}(\hat{r})$ are the generalized spherical harmonics. The radial wave functions in the above equations are generated numerically using the T-matrix constructed from the appropriate potentials and are given as follows

$$\begin{aligned} [\psi_{\Lambda N}^{(-)*}]_{L'_F S'_F, L_F S_F}^J(p_F, r) &= j_{L_F}(p_F) \delta_{L_F L'_F} \delta_{S_F S'_F} \\ &\quad + \int \frac{p'^2 dp' \langle p_F(L_F S_F) J | T_{\Lambda N \rightarrow \Lambda N} | p'(L'_F S'_F) J \rangle}{E_N(p_F) + E_\Lambda(p_F) - E_N(p') - E_\Lambda(p') + i\eta} j_{L'_F}(p' r) \end{aligned} \quad (28)$$

$$\begin{aligned} [\psi_{NN}^{(+)}]_{L'_I S_I, L_I S_I}^J(p_I, r) &= j_{L_I}(p_I) \delta_{L_I L'_I} \\ &\quad + \int \frac{p'^2 dp' \langle p'(L'_I S_I) J | T_{NN \rightarrow NN} | p_I(L_I S_I) J \rangle}{2E_N(p_I) - 2E_N(p') + i\eta} j_{L'_I}(p' r). \end{aligned} \quad (29)$$

FIGURES

FIG. 1. Feynman diagram for the $np \rightarrow \Lambda p$ reaction

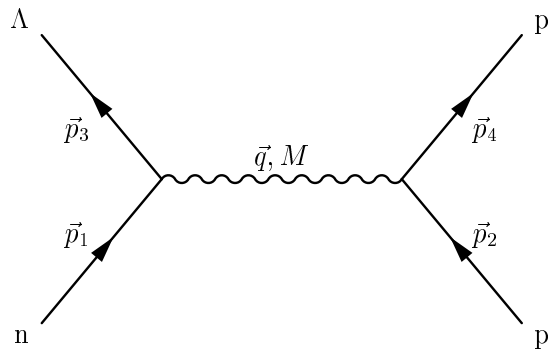


FIG. 2. Total cross sections for the reaction $pn \rightarrow p\Lambda$ as a function of the proton lab momentum using the weak one-pion-exchange potential. Dashed line: calculation omitting form factors and strong correlations; thin solid line: including form factors and NN initial correlations; thick solid line: including form factors and both NN and ΛN distortions.

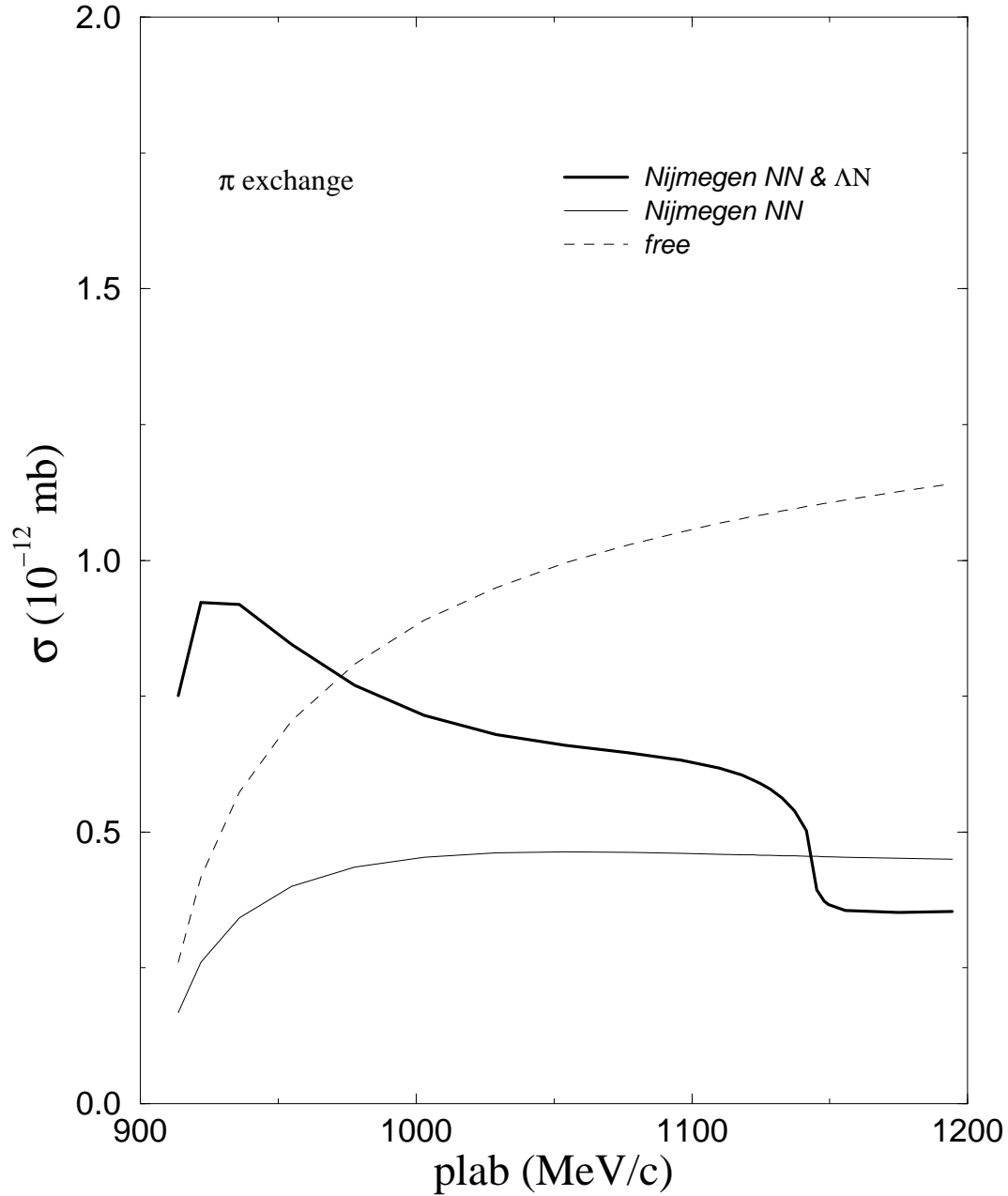


FIG. 3. Total cross sections for the reaction $pn \rightarrow p\Lambda$ as a function of the proton lab momentum. The strong distortions are generated with the NN Nijmegen 93 and YN Nijmegen Soft Core models (a) or by the NN Bonn B and YN Jülich A (b). Dashed line: π -exchange only; thin solid line: $\pi + \rho$; thick solid line: full set of mesons.

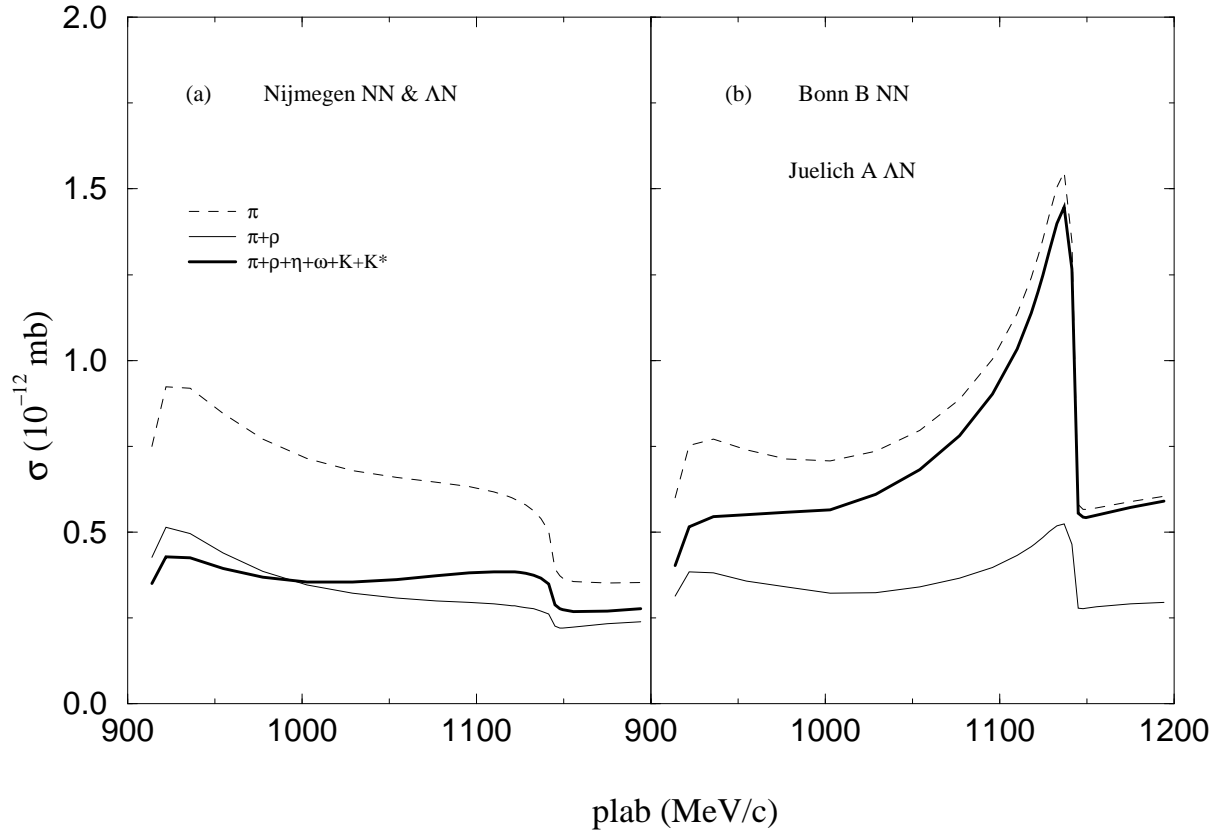


FIG. 4. Different partial wave contributions to the cross section for the $pn \rightarrow p\Lambda$ reaction. Only the pion is considered in the weak transition potential. The NN and ΛN distorted waves are generated with the Nijmegen models (a) and the Bonn B and Jülich A models (b) respectively.

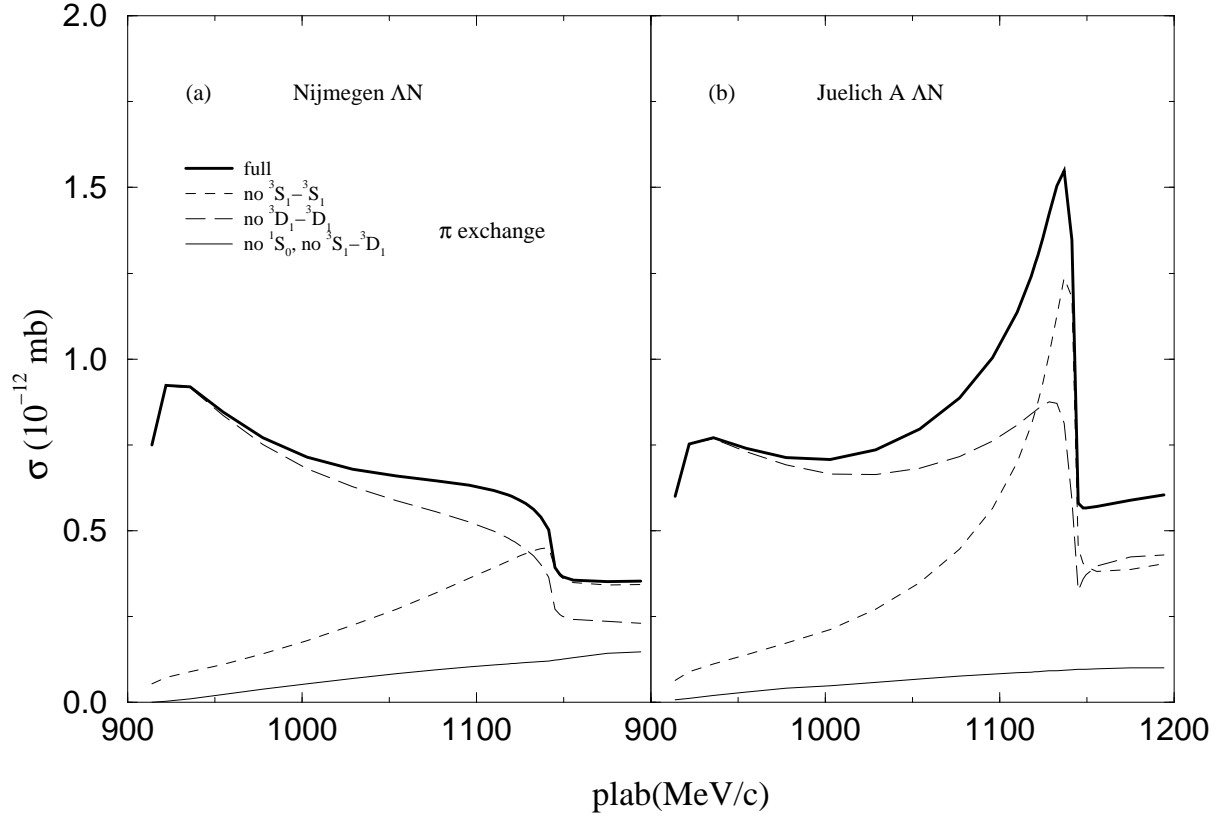


FIG. 5. Differential cross sections in the center of mass for the reaction $pn \rightarrow p\Lambda$ at $p_{\text{lab}} = 1137$ MeV/c. Dashed line: π -exchange only; thin solid line: $\pi + \rho$; thick solid line: full set of mesons. The NN and ΛN wave functions are generated using Bonn B and Jülich A models respectively.

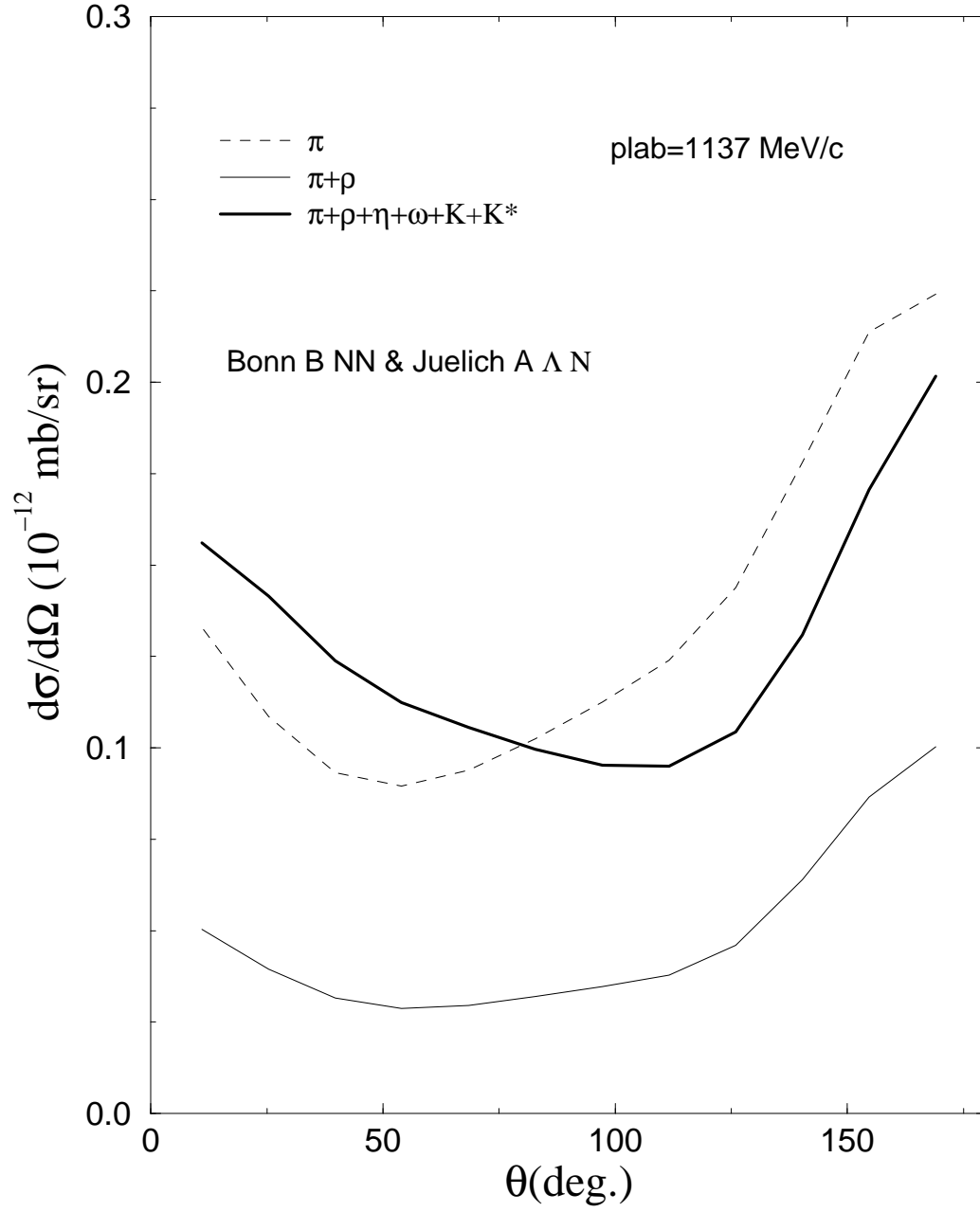


FIG. 6. Total asymmetry A for the reaction $pn \rightarrow p\Lambda$ as a function of the proton lab momentum using the weak one-pion-exchange potential. Dashed line: calculation omitting form factors and strong correlations; thin solid line: including form factors and NN distortions; thick solid line: including form factors and both NN and ΛN distortions.

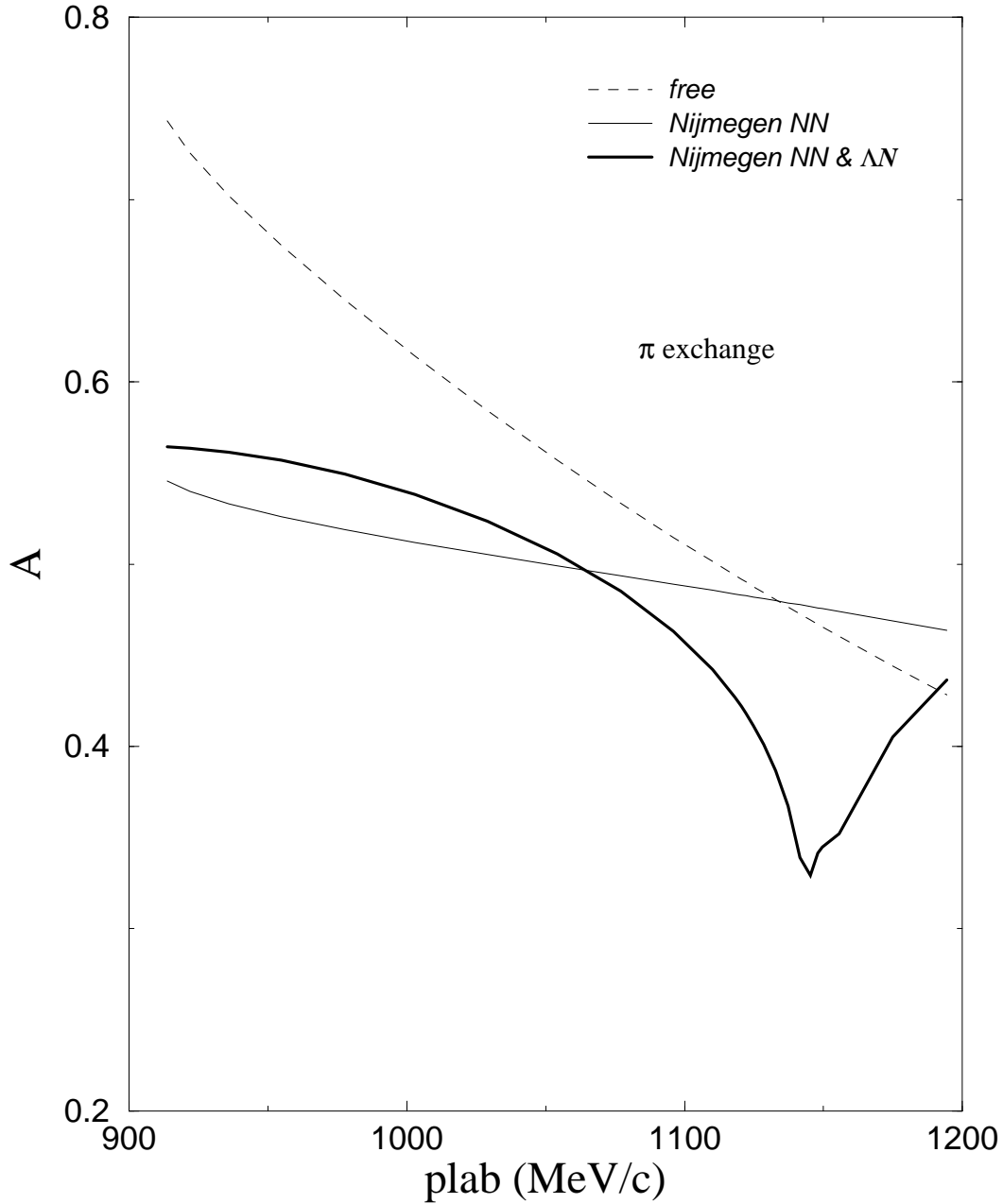


FIG. 7. Total asymmetry for the reaction $pn \rightarrow p\Lambda$ as a function of the proton lab momentum. The NN and ΛN distortions are generated with the Bonn B and Jülich A potentials respectively. Dashed line: π -exchange only; thin solid line: $\pi + \rho$; thick solid line: full set of mesons.

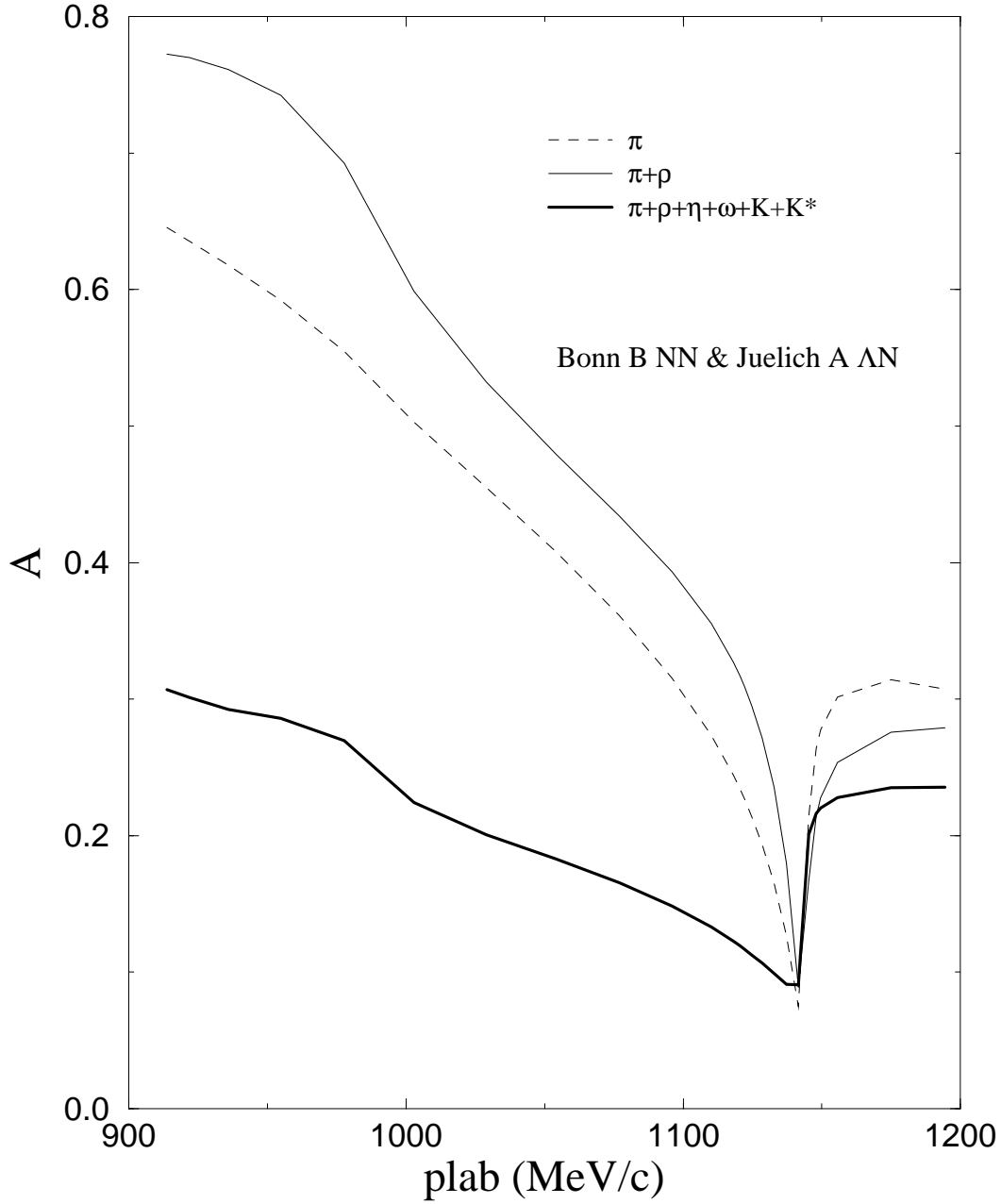
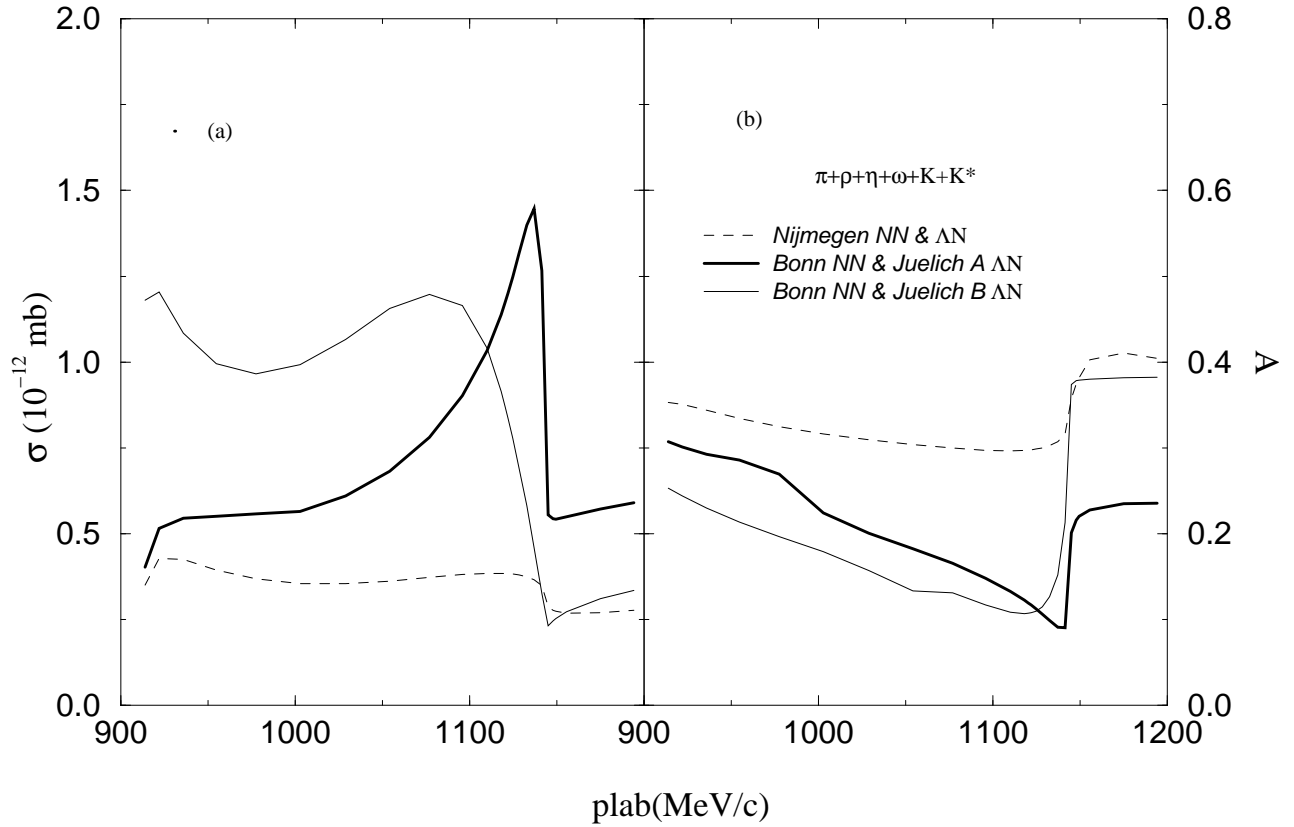


FIG. 8. Total cross section (a) and asymmetry (b) for the reaction $pn \rightarrow p\Lambda$ as a function of the proton lab momentum using the full meson-exchange weak transition potential with various strong potential models. Dashed line: NN Nijmegen 93 and YN Nijmegen soft-core; thin solid line: NN Bonn B and YN Jülich B; thick solid line: NN Bonn B and YN Jülich A.



TABLES

TABLE I. Constants appearing in weak transition potential for the different mesons.

μ_i	$K_C^{(i)}$	$K_{SS}^{(i)}$	$K_T^{(i)}$	$K_{PV}^{(i)}$
π	0	$\frac{B_\pi}{2\bar{M}} \frac{g_{NN\pi}}{2M}$	$\frac{B_\pi}{2\bar{M}} \frac{g_{NN\pi}}{2M}$	$A_\pi \frac{g_{NN\pi}}{2M}$
η	0	$\frac{B_\eta}{2\bar{M}} \frac{g_{NN\eta}}{2M}$	$\frac{B_\eta}{2\bar{M}} \frac{g_{NN\eta}}{2M}$	$A_\eta \frac{g_{NN\eta}}{2M}$
K	0	$\frac{1}{2M} \frac{g_{\Delta NK}}{2\bar{M}}$	$\frac{1}{2M} \frac{g_{\Delta NK}}{2\bar{M}}$	$\frac{g_{\Delta NK}}{2M}$
ρ	$g_{NN\rho}^V \alpha_\rho$	$2 \frac{\alpha_\rho + \beta_\rho}{2\bar{M}} \frac{g_{NN\rho}^V + g_{NN\rho}^T}{2M}$	$-\frac{\alpha_\rho + \beta_\rho}{2\bar{M}} \frac{g_{NN\rho}^V + g_{NN\rho}^T}{2M}$	$-\varepsilon_\rho \frac{g_{NN\rho}^V + g_{NN\rho}^T}{2M}$
ω	$g_{NN\omega}^V \alpha_\omega$	$2 \frac{\alpha_\omega + \beta_\omega}{2\bar{M}} \frac{g_{NN\omega}^V + g_{NN\omega}^T}{2M}$	$-\frac{\alpha_\omega + \beta_\omega}{2\bar{M}} \frac{g_{NN\omega}^V + g_{NN\omega}^T}{2M}$	$-\varepsilon_\omega \frac{g_{NN\omega}^V + g_{NN\omega}^T}{2M}$
K*	$g_{\Delta NK^*}^V$	$2 \frac{1}{2M} \frac{g_{\Delta NK^*}^V + g_{\Delta NK^*}^T}{2\bar{M}}$	$-\frac{1}{2M} \frac{g_{\Delta NK^*}^V + g_{\Delta NK^*}^T}{2\bar{M}}$	$-\frac{g_{\Delta NK^*}^V + g_{\Delta NK^*}^T}{2M}$

REFERENCES

- [1] R. Feynman and M. Gell-Mann, Phys. Rev. **109**, 193 (1958).
- [2] C.S. Wood et al, Science **275**, 1759 (1997).
- [3] E. Adelberger and W. Haxton, Ann. Rev. Nucl. Part. Sci. **35**, 501 (1985).
- [4] A. Parreño, A. Ramos, and C. Bennhold, Phys. Rev. C **56**, 339 (1997).
- [5] T. Kishimoto, *Weak and electromagnetic interactions in nuclei*, Eds. H. Ejiri, T. Kishimoto and T. Sato, World Scientific (1995) 514.
- [6] V.G. Stoks, R.A.M. Klomp, C.P.F. Terheggen and J.J. de Swart, Phys. Rev. C **49**, 2950 (1994).
- [7] *Computational Nuclear Physics 2. Nuclear Reactions*, Eds. K. Langanke, J.A. Maruhn and S.E. Koonin, Springer-Verlag (1993) 1-29.
- [8] P.M.M. Maessen, Th. A. Rijken and J.J. de Swart, Phys. Rev. C **40**, 2226 (1989).
- [9] B. Holzenkamp, K. Holinde, and J. Speth, Nucl. Phys. **A500**, 485 (1989).
- [10] J. Haidenbauer, K. Holinde, K. Kilian, T. Sefzick and A.W. Thomas, Phys. Rev. C **56**, 3496 (1995).
- [11] Y.Yamamoto, R. Reuber, H. Himeno, S. Nagata and T. Motoba, Czec. Jour. Phys. **42**, 1249 (1992).
- [12] Y.Yamamoto, T. Motoba, H. Himeno, K. Ikeda and S. Nagata, Prog. Theor. Phys. **Suppl. 117**, 361 (1994).
- [13] M. Hjorth-Jensen, A. Polls, A. Ramos and H. Mütter, Nucl. Phys. **A605**, 458 (1996).